Estimation of Frequency Offset In Mobile Satellite Modems

W.G. Cowley†, M. Rice and A.N. McLean
Digital Communications Group
University of South Australia
The Levels, Pooraka, South Australia 5095
fax +61-8-302 3873
†(Currently at the Communications Research Centre, Ottawa
and the University of Ottawa, Electrical Engineering Dept.)

Abstract

In mobilesat applications, frequency offset on the received signal must be estimated and removed prior to further modem processing. A straightforward method of estimating the carrier frequency offset is to raise the received MPSK signal to the $M-$th power, and then estimate the location of the peak spectral component. An analysis of the lower signal to noise threshold of this method is carried out for BPSK signals. Predicted thresholds are compared to simulation results. It is shown how the method can be extended to π/M MPSK signals. A real-time implementation of frequency offset estimation for the Australian mobile satellite system is described.

1 Introduction

Frequency uncertainty in mobile satellite applications arises from doppler offsets due to vehicle motion or local oscillator drift. As the symbol rate r_s is usually low, the frequency offset can be a substantial fraction of r_s and must be removed prior to receive filtering and carrier or timing synchronisation.

A number of previous approaches have used frequency offset detectors in a feedback loop to correct for frequency shifts e.g. [1]. Relatively little attention has been given to feedforward estimators which operate over a block of symbols. In burst mode applications where rapid acquisition is important, the feedforward form of estimation is desirable.

Estimation of the frequency offset during carrier only or preamble portions of the received signal is easier than when modulation is present. Most of this paper concerns the case when random BPSK or QPSK symbols are transmitted. Estimation of the frequency offset with carrier is examined in [2].

A relatively simple form of estimating the frequency offset involves stripping the modulation by raising the MPSK signal to the $M-$th power, and then estimating the location of the resulting spectral peak via the Fast Fourier Transform (FFT) algorithm. This will be called the FFT method. Other forms of nonlinearity may be used for removing the modulation (e.g. [3]), but only the $M-$th power operation is considered in this paper.

The frequency resolution of the FFT method is limited by the the duration of the received signal. However it is possible to improve the accuracy of locating a single spectral component by interpolating between the largest bins, or by evaluating the Discrete Fourier Transform iteratively to locate the spectral peak. In practice, small errors in the frequency estimate (e.g. less than 1% of r_s) may not matter since they can be removed during carrier phase recovery.

An interesting alternative to the FFT method has been reported in [4]. This technique effectively estimates the autocorrelation function of the $M-$th power signal at selected lags and uses this to efficiently estimate the spectral peak location.

Section 2 analyses the FFT method for BPSK, in order to predict the probability of failure. In section 3, simulated results are compared to the predicted results for BPSK. In addition simulations of QPSK are presented. In section 4 a modified version of the FFT method is described which can be used with π/M versions of MPSK. Finally, section 5 presents a summary of the real-time implementation of frequency estimation and signal detection strategies for preamble and message signals.

2 Threshold Analysis for the FFT Method

An important question concerning the FFT method of frequency offset estimation is when the technique is likely to fail due to a noise peak in the FFT being larger than the desired signal peak. In this case, since the offending noise peak may occur at any bin in the FFT

C-6

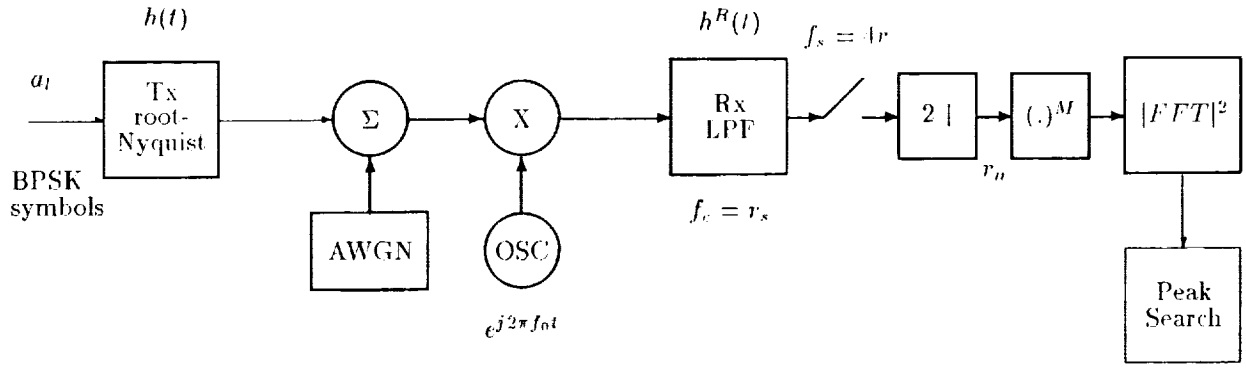

Figure 1: Baseband Signal Model for FFT Method of Frequency Offset Estimation

output, the resulting estimate is effectively a uniformly distributed random variable with no correlation to the actual offset. The probability of failure is primarily a function of the E_b/N_0 , the number of symbols used, and the signal constellation size M. This failure threshold is analysed for BPSK signals in this section.

The signal model employed is shown in Figure 1. Thick lines indicate complex-valued quantities. Standard square-root raised-cosine transmit filtering is assumed, with transmit filter impulse response $h(t)$. At the receiver, frequency estimation must be carried out before normal receive filtering since the frequency offset may be a substantial fraction of the symbol rate. In this model an ideal filter with twice the normal bandwidth is used, i.e. $f_c = r_s$ Hz, prior to frequency estimation. It is assumed that the filtered signal is sampled and then decimated by a factor of 2, to two samples per symbol period T. This is the minimum possible sampling rate, and furthermore ensures that the noise samples are independent which makes the following analysis tractable. The use of 2 samples per T, allows a frequency offset f_o of up to $\pm r_s/4$, for example, for QPSK, or twice this amount for BPSK. The effect of not decimating the signal, and using 4 samples per T, is investigated by simulation in section 3 and found to be quite similar to the minimum sampling-rate case under discussion.

Received signal samples before the squarer can be expressed

$$r_n = s_n + w_n \tag{1}$$

with the signal component s_n

$$s_n = e^{j2\pi f_o n 2T_s} \sum_k a_k h(\tau + n2T_s - kT) \tag{2}$$

where a_k is the $k-$th transmitted symbol $= \pm 1$, T_s is the initial sampling period $= T/4$ and τ is an arbitrary time offset. The signal samples are taken without timing recovery or matched filtering and so contain significant InterSymbol Interference (ISI). The squared signal is a "noisy" complex exponential; this section assumes that the random components in s_n^2 are uncorrelated and small compared to the thermal noise terms. These assumptions appear to be justified at low signal to noise ratios. σ_S^2 will denote $E\{|s_n|^2\} = E_b/4$. The zero-mean complex-valued noise samples w_n have real and imaginary parts whose variance will be denoted σ_R^2 equal to $N_0/4$.

Consider now the power estimates from the Discrete Fourier Transform of N received samples raised to the $M-$th power i.e. $r_0^2, r_1^2 \cdots r_{N-1}^2$. Let

$$P_m = \left| \sum_{n=0}^{N-1} (s_n + w_n)^2 e^{-j2\pi nm/N} \right|^2 \tag{3}$$

for $m = 0, \cdots N-1$ Let the bin containing the signal peak be at $m = m_S$; this value of P_m will be denoted P_S. The other bins contain independent noise power estimates. Any noise bin ($m \neq m_S$) will be denoted P_N.

To determine the mean value of the noise power estimates, from the last equation

$$E\{P_N\} = E\left\{ \sum_p \sum_q (s_p + w_p)^2 (s_q^* + w_q^*)^2 \right. \\ \left. e^{-j2\pi m(p-q)/N} \right\} \text{ for } m \neq m_S \tag{4}$$

where $*$ denotes complex conjugate. The only non-zero terms in this expression arise from one of the signal times noise components and the noise-only components.

The former term is

$$E\{\sum_p \sum_q 4 s_p w_p s_q^* w_q^* e^{-j2\pi m(p-q)/N}\}$$

which, remembering that the noise samples are independent, simplifies to

$$\sum_p 4E\{|s_p|^2\}E\{|w_p|^2\} = 8N\sigma_S^2\sigma_R^2$$

and the latter term is

$$E\{\sum_p \sum_q w_p^2 w_q^{*2} e^{-j2\pi m(p-q)/N}\}$$

which simplifies to, using $E\{x^4\} = 3\sigma_x^4$ when x is $N(0, \sigma_x^2)$

$$\sum_p E\{|w_p|^4\} = 8N\sigma_R^4$$

The final result is

$$E\{P_N\} = 8N(\sigma_S^2\sigma_R^2 + \sigma_R^4) \quad (5)$$

Space does not permit a full derivation of the mean and variances of P_S and P_N in this paper. Proceeding in a similar fashion to that illustrated above, the following results are obtained:

$$\sigma_{P_N} = E\{P_N\} \quad (6)$$

$$E\{P_S\} = N^2\sigma_S^4 + E\{P_N\} \quad (7)$$

$$\sigma_{P_S}^2 = \sigma_{P_N}^2 + 16N^3\sigma_R^2\sigma_S^4(\sigma_S^2 + \sigma_R^2) \quad (8)$$

These results assume that terms of order N have been neglected from the variance expressions.

In order to compute the probability that $P_N > P_S$ we need to know the density functions of P_N and P_S. These distributions are not obvious due to the non-linear operation before the FFT. However it may be observed that (5) to (8) correspond exactly to the expressions for mean and variance of chi-square and non-central chi-square distributions (e.g. [5] (1.1.109) and (1.1.122)) each with 2 degrees of freedom. Using these distributions

$$p_{P_N}(p_N) = \frac{1}{2\sigma^2} e^{-p_N/2\sigma^2} \text{ for } p_N \geq 0 \quad (9)$$

$$p_{P_S}(p_S) = \frac{1}{2\sigma^2} e^{-(s^2+p_S)/2\sigma^2} I_0(\sqrt{p_S}s/\sigma^2) \text{ for } p_S \geq 0 \quad (10)$$

where $2\sigma^2 = E\{P_N\}$, $s^2 = N^2\sigma_S^4$ and $I_0()$ is the zero-th order modified Bessel function of the first kind.

Let p_F denote the fail probability when any $P_N > P_S$. Then

$$p_F = 1 - \text{ prob(all } P_N < P_S)$$

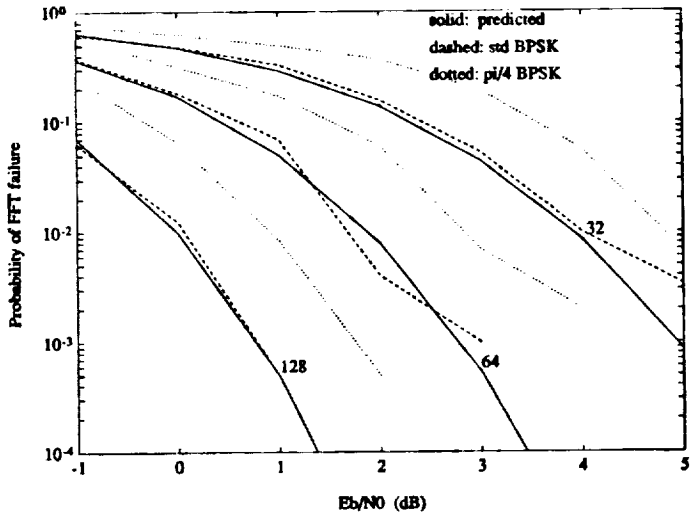

Figure 2: Failure Probability for BPSK Signals

For a given value p_S, of P_S, since the P_N are independent,

$$\text{prob(all } P_N < p_S) = \left(\int_0^{p_S} p_N(p_N)dp_N\right)^{N-1} = \left(1 - e^{-p_S/2\sigma^2}\right)^{N-1}$$

and so

$$p_F = 1 - \int_0^{\infty} \left(1 - e^{-p_S/2\sigma^2}\right)^{N-1} p_{P_S}(p_S)dp_S \quad (11)$$

When (10) is substituted into (11), the failure probability may be integrated numerically.

From here it is easy to predict the variance of the resulting errors in the frequency estimate $\hat{f}_o$. Letting $\Delta f_o = \hat{f}_o - f_o$, as Δf_o is uniformly distributed, with either $|\Delta f_o| < f_s/2$ when the FFT fails, else $|\Delta f_o| < f_s/2N$, gives

$$\sigma_{\Delta f_o}^2 = \frac{1}{12}\left((\frac{f_s}{2})^2 p_F + (\frac{f_s}{2N})^2(1 - p_F)\right) \quad (12)$$

where N is the FFT size.

3 Simulation Results for the FFT Method

The signal model in Figure 1 was simulated in order to check the predicted FFT thresholds derived in section 2. A normalised symbol rate of 1 symbol per second was used. The continuous-time signals in Figure 1 were simulated with 4 samples per T. The excess bandwidth parameter in the transmit filter was 40%.

During the simulations, packets of random bits were generated and a random frequency offset between

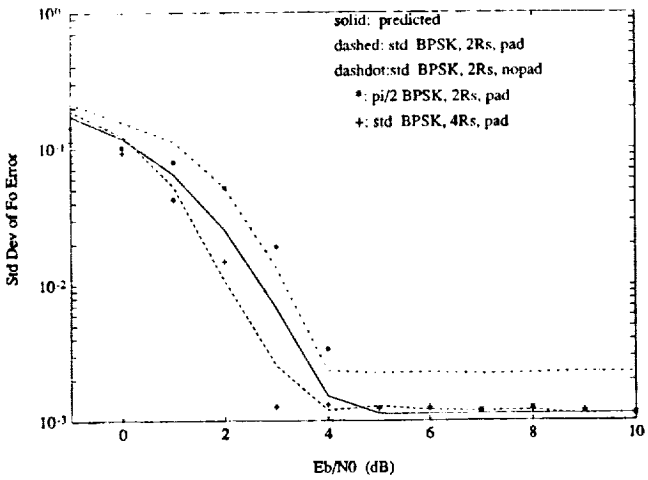

Figure 3: Frequency Accuracy for 64 BPSK Symbols

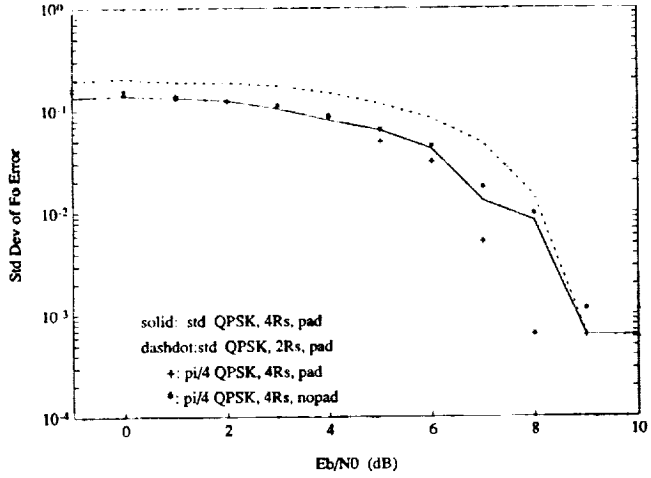

Figure 4: Frequency Accuracy for 64 QPSK Symbols

$\pm r_s/4$ was added. The FFT size was twice the number of symbols received, without any zero padding of the data samples and with the decimation shown in Figure 1. When the data was zero padded with an equal length of zeros, the FFT was four times the number of symbols. The zero padding gives improved performance since it reduces the signal loss caused by frequency offsets at non-integer multiples of the initial frequency resolution, and the frequency accuracy is improved. It could be argued that the effective number of independent noise bins in the FFT output is the same (N) with or without zero padding; this seems to be supported by simulation.

Figure 2 shows a plot of FFT failure probability for 32, 64 and 128 bit BPSK signals. The predicted values from (11) are plotted with solid lines. These simulations used twice oversampling (i.e. 2 samples per T) and zero padding. (Since the analysis effectively assumes bin-centred doppler frequencies, the use of zero padding is appropriate to remove most of the loss due to random frequency offsets.) The figure shows fairly good agreement between the predicted and measured results for BPSK. The lack of simulation results at low values of p_F reflects the difficulty in simulating rare FFT failures at high signal to noise ratios. Plots for $\pi/2$ BPSK are discussed in the next section.

In Figure 3 the standard deviation of the frequency error Δf_o is plotted for 64 bit BPSK signals and compared to the predicted value from section 2. In the evaluation of (12), N was doubled for comparison with simulations using zero padding. All the simulations show approximately similar thresholds in the vacinity of $E_b/N_0 = 4$ dB, below which the frequency error increases rapidly as the failure probability becomes significant. It can be seen that twice oversampling without padding gives slightly worse results, as expected.

Four times oversampling, with padding, has been included for comparison. In this case the noise samples are correlated and the noise spectrum is no longer flat, as it is for section 2. Notice that the final accuracy, above threshold, is the same as two samples per T with padding, as expected.

Figure 4 shows 64 symbol QPSK simulations of frequency accuracy using the FFT method. Again the vertical scale is relative to $r_s = 1$ symbol/sec. The threshold is significantly higher than the $M = 2$ case (almost 6 dB). Again the thresholds for $2r_s$ or $4r_s$ sample rates appear to be similar, and the advantages of padding can be seen.

Reliable frequency estimation below the thresholds shown in figures 3 and 4 could be obtained by using more symbols per FFT, or by combining results from separate FFTs (see section 5).

4 Frequency Estimation for π/M MPSK

Variants of MPSK modulation such as $\pi/2$ BPSK (or Aviation BSPK) and $\pi/4$ QPSK can readily be handled by the FFT method of frequency offset estimation. These modulation schemes are now used in some mobile satellite systems (e.g. [6]). They rotate alternate symbols by π/M radians which reduces the amplitude variations in the transmitted signal.

The effect of these symbol rotations can be appreciated as follows. Suppose that the receive signal has been ideally filtered and sampled at one sample per T with no ISI or thermal noise present. The sampled signal could be written

$$a_0,\ a_1 e^{j\pi/M} e^{j\delta},\ a_2 e^{j2\delta},\ a_3 e^{j\pi/M} e^{j3\delta}, \ldots$$

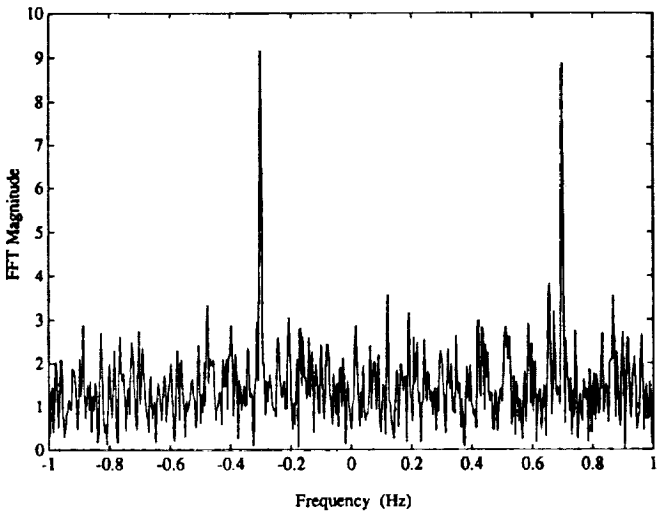

Figure 5: Sample Power Spectrum for $\pi/2$ BPSK

where $\delta = 2\pi f_o T$ represents the phase change per symbol period due to frequency shift. After the $M-$th power operation the samples become

$$a_0^M,\ a_1^M e^{j\pi} e^{jM\delta},\ a_2^M e^{j2M\delta},\ a_3^M e^{j\pi} e^{j3M\delta}, \cdots$$

If $a_k \in e^{j2\pi/M}, k = 0, 1, \cdots M-1$, then $a_k^M = 1$ so the previous sequence can be written

$$1,\ -e^{jM\delta},\ e^{j2M\delta},\ -1e^{j3M\delta},\ \cdots$$

This represents a discrete-time complex exponential, whose frequency is M times the original f_o, which has been modulated by a sequence of alternating sign, $\cdots 1, -1, 1, -1 \cdots$, of period $r_s/2$. (The MPSK case would be the same except for the alternating signs.) The signal spectral component is therefore split into two discrete components, separated from Mf_o Hz by $\pm r_s/2$.

In the practical case with more than one sample per symbol period and ISI and/or noise, the effect in the frequency domain is similar. Figure 5 shows a typical spectral estimate from the FFT method for 128 bits of $\pi/2$ BPSK at E_b/N_0 = 6dB. The frequency offset was 10% of r_s; two components can therefore be seen at $0.2r_s \pm r_s/2$. It can be observed that the noise spectrum is flat as 2 samples per T were used in this simulation.

In order to estimate the frequency offset for π/M MPSK signals, the peak sum of FFT bins separated by r_s Hz can be located. This is a straightforward extension of the normal peak search method for MPSK. At this stage the analysis described in section 2 has not been extended to $\pi/2$ BPSK, although this should be possible. Some simulation results for π/M MPSK are shown in figures 2, 3 and 4. The higher failure probability in figure 2 might be expected due to the spectral peak splitting and consequent lower noise immunity. The $\sigma_{\Delta f_o}$ thresholds are slightly higher for $\pi/2$ BPSK, although this appears to be reversed for $\pi/4$ QPSK with four times oversampling. Further simulations would be necessary for precise location of these thresholds since a very small number of FFT failures can significantly effect the shape of the frequency error in the threshold region.

5 Real-Time Implementation

A real time implementation of a frequency estimator was required for use in mobilesat(TM) mobile terminals. The mobile terminals are required to acquire phase acquisition of a 3300 symbols/sec $\pi/4$ QPSK voice activated carrier using a 40ms preamble, or else, assuming loss of the preamble, (due to blockages, fading etc.), within 180ms. In addition, initial acquisition must be obtained using a continuous transmission (during "Call Set Up" mode) within 120ms with a 500Hz frequency offset. These acquisition times are specified at E_b/N_0 of 6dB. Refer to [6] for details.

Two methods were developed to meet these specifications. These incorporated detection, frequency estimation, timing estimation and then phase estimation, in that order. In the case of the preamble, the signal was designed to have two discrete components. This allowed a very reliable and efficient PSD correlation method to be used for detection, frequency and timing estimation. To summarise, four times oversampled data was used, and an FFT length of 256 was chosen, giving a bin width of 51.6Hz. Detection was based on comparison of a peak to average bin correlation ratio with a threshold. A detection threshold was chosen by experiment. This gave 100% correct detects at values of E_b/N_0 down to 3dB. To obtain better resolution than the bin width, an interpolation method was used between bins. This gave a worst case RMS frequency estimate error was of about 6.7Hz, and typically less than 3Hz at 3dB. Running on a 50MHz DSP32C, this required a processing time of 855ms per estimate, and an update rate of every 8 symbols (2.4ms) was chosen. This resulted in measured total carrier acquisition times (ie including detection, frequency timing and phase recovery) of less than 27ms (typically about 26ms) at E_b/N_0 of 6dB. About 10ms of this is due to filtering and phase recovery delays.

In the case of the preambleless (i.e. random data) signal acquisition, the $M = 4$ FFT method was used. As with the preamble case, four samples per symbol period and a 256 length FFT was used without padding (i.e. 64 symbols). This gave an equivalent bin width of 12.8Hz (0.0039 relative to r_s), although using interpolation the frequency resolution could be made much less. Frequency errors of 10.3Hz maximum and 3.8Hz typically at Eb/No of 3dB were recorded, which were

considered acceptable given the lock range of the phase recovery technique.

The variance of the signal to noise ratio estimate was found to be too high to produce a reliable detection/rejection rule when compared with a detection threshold. To improve this, the FFT output was lowpass filtered to suppress spurious components from causing erroneous detections. In addition, hysteresis was built into the detection process, to prevent premature detection of signals i.e. before the FFT input buffer had sufficient samples of an unfaded signal to produce an accurate frequency estimate. These two enhancements allowed a trade-off between reliability and detection time to be made. This was done experimentally to meet the mobilesat specifications, and produce very reliable detection and estimation. Total processing delay per frequency estimate was 1050ms and an update rate of 8 symbols was chosen. The typical times for carrier acquisition were measured to be about 80ms at 6dB.

At lower values of E_b/N_0 , the detection time was increased although the 120ms specification was still easily met at 3dB. Detection failure was set at about 1.5dB. Signals with lower E_b/N_0 are too noisy to be useful in the given application.

A crucial performance parameter in the random data frequency estimation technique was the input noise bandwidth. Due to the high tolerable frequency offsets (< 1500Hz) the received signal was digitally filtered using a low pass filter with cut-off at 1.25 times the symbol rate (i.e. slightly larger than in sections 2 to 4). This was found to give good performance under all conditions, although improvements could be attained with tighter filtering.

6 Conclusions

A method of analysing the lower E_b/N_0 threshold for the $M-$th power method of frequency estimation for BPSK signals has been presented. Simulations show reasonable agreement with the predicted probability of the wrong FFT peak being chosen. The FFT method can be readily be adapted to π/M MPSK signals, with a small loss in performance for $\pi/2$ BPSK. Sample simulations for BPSK and QPSK signals give some idea of the effects of oversampling and zero padding on the FFT threshold. An implementation of the FFT method, and related processing, has been tested in real-time operation, and optimised on mobile satellite channels. This includes using the results of multiple transforms, rather than one large one, to produce reliable estimation and detection at the required operating point.

Acknowledgements

The authors would like to acknowledge the support of The Australian Space Office and Optus Communications in the implementation aspects of this work. The first author thanks Dr. Stewart Crozier of the CRC in Ottawa for useful discussions regarding frequency estimation.

References

[1] T. Alberty , V. Hespelt and H. Gockler, "A Digital Multicarrier Demodulator with Fast Synchronisation for Mobile SCPC Satellite Communications", *Proc. ICDSC-8*

[2] D. Rife and R. R. Boorstyn, " Single-Tone Parameter Estimation from Discrete-Time Observations", *IEEE Trans. Inform. Theory*, Vol. IT-20, No. 5, Sept. 74.

[3] A. J. Viterbi and A. M. Viterbi, "Nonlinear Estimation of PSK-Modulated Carrier Phase with Applications to Burst Digital Transmission", *IEEE Trans. Inform. Theory*, Vol. IT-29, No. 4, July, 1983

[4] S. N. Crozier and K. W. Moreland "Performance of a Simple Delay-Multiply-Average Technique for Frequency Estimation", Proc. *Canadian Conf. on Elec. and Comp. Eng.*, Toronto, Sept. 1992

[5] J. G. Proakis, *"Digital Communications"*, 2nd Ed, McGraw-Hill, 1989

[6] "User Terminals for Accessing the Mobilesat Satellite Communications System", *Standards Australia*. AS 4080, 1992